

Linköping Studies in Science and Technology
Licentiate Thesis No. 1561

Me-Si-C (Me= Nb, Ti or Zr)

Nanocomposite and Amorphous

Thin Films

Olof Tengstrand



Linköping University
INSTITUTE OF TECHNOLOGY

LIU-TEK-LIC-2012:46
Thin Film Physics Division
Department of Physics, Chemistry and Biology (IFM)
Linköping University
SE-581 83 Linköping, Sweden

© Olof Tengstrand 2012
ISBN: 978-91-7519-730-2
ISSN: 0280-7971
Printed by LiU-Tryck
Linköping, Sweden, 2012

Abstract

This thesis investigates thin films of the transition metal carbide systems Ti-Si-C, Nb-Si-C, and Zr-Si-C, deposited at a low substrate temperature (350 °C) with dc magnetron sputtering in an Ar discharge. Both the electrical and mechanical properties of these systems are highly affected by their structure. For Nb-Si-C, both the ternary Nb-Si-C and the binary Nb-C are studied. I show pure NbC films to consist of crystalline NbC grains embedded in a matrix of amorphous carbon. The best combination of hardness and electrical resistivity are for ~15 at.% a-C phase. The properties of nc-NbC/a-C are similar to films consisting of nc-TiC/a-C. I further show that in a model system of epitaxial TiC_x ($x \sim 0.7$) up to 5 at.% Si can be incorporated. At higher Si content, Si starts segregate out from the TiC_x to the grain boundaries causing a loss of epitaxy. Higher amounts of Si into the Nb-Si-C and Zr-Si-C systems make them become amorphous. These amorphous structures are unstable under electron irradiation were they crystallize. I show that the cause of crystallization is driven by atomic displacement events.

Preface

I here present the outcome of my first three years of work as a PhD-student in the Thin Film Group at Linköping University. The licentiate thesis has been made within Theme 1 of the VINN Excellence Center on Functional Nanoscale Materials (FunMat). The research was carried out in cooperation with Uppsala University, Technical Research Institute of Sweden (SP), and the companies Impact Coatings AB and ABB AB.

Included papers

Incorporation effects of Si in TiC_x thin films

O. Tengstrand, N. Nedfors, U. Jansson, A. Flink, P. Eklund, L. Hultman.

Manuscript in preparation

Beam-induced crystallization of Me-Si-C (Me= Nb or Zr) thin films during transmission electron microscopy

O. Tengstrand, N. Nedfors, M. Andersson, J. Lu, U. Jansson, A. Flink, P. Eklund, L. Hultman

Manuscript in preparation

Structural, mechanical and electrical-contact properties of nanocrystalline-NbC/amorphous-C coatings deposited by magnetron sputtering

N. Nedfors, **O. Tengstrand**, E. Lewin, A. Furlan, P. Eklund, L. Hultman, U. Jansson

Surface and Coatings Technology, 206, 354-359 (2011)

Related papers not included in the thesis

Phase-stabilization and substrate effects on nucleation and growth of $(Ti,V)_{n+1}GeC_n$ thin films

S. Kerdsonpanya, K. Buchholt, **O. Tengstrand**, J. Lu, J. Jensen, L. Hultman, P. Eklund

Journal of Applied Physics, 110, 053516 (2011)

Discovery of the Ternary Nanolaminated Compound Nb_2GeC by a Systematic Theoretical-Experimental Approach

P. Eklund, M. Dahlqvist, **O. Tengstrand**, L. Hultman, J. Lu, N. Nedfors, U. Jansson, J. Rosén

Physical Review Letters 109, 035502 (2012)

Acknowledgements

Lots of people have in different ways helped and supported me during my time in the thin film physics group. I hope you all find your rightful place in the list below.

I would like to thank:

* My supervisor, Lars Hultman, and co-supervisor, Per Eklund. You have been a great help.

* Nils Nedfors and Ulf Jansson at Uppsala University

* The persons from ABB, Impact coatings and SP involved in my projects in FunMat Theme 1. A special thanks to Axel Flink, who always seems to find a little bit of time to help me and since the spring 2012 also is my co-supervisor.

* Co-authors, for a fruitful discussions and good ideas.

* Colleagues, for cheering me up, reminding me to take breaks, help and interesting discussions in both work and non-work related topics.

* Sara and my family for support.

Contents

Abstract.....	i
Preface.....	iii
Included papers.....	v
Acknowledgements.....	vii
1 Introduction	1
2 Electrical contacts.....	3
3 Material systems	7
3.1 Me-C	7
3.2 Me-Si-C.....	8
4 Deposition process	11
4.1 Magnetron sputtering	11
5 Characterization	15
5.1 Transmission electron microscopy (TEM).....	15
5.1.1 <i>Imaging</i>	15
5.1.2 <i>Energy-dispersive X-ray Spectroscopy (EDX)</i>	17
5.1.3 <i>Sample preparation</i>	18
5.2 X-ray diffraction (XRD)	19
5.2.1 <i>Bragg's law</i>	19
5.2.2 <i>Examples of different methods in X-ray diffraction</i>	19
5.2.3 <i>Strain measurements (sin²ψ-method)</i>	21
5.3 X-ray photoelectron spectroscopy (XPS).....	23
6 Electron radiation damages in TEM.....	25
6.1 Damages caused by elastically scattered electrons	25
6.2 Damages caused by inelastic electron scattering.....	27
6.2.1 <i>Specimen heating</i>	27
6.2.2 <i>Radiolysis</i>	27
7 Summary of papers	29
7.1 Paper I	29
7.2 Paper II.....	29
7.3 Paper III	30
8 Future work.....	31
Paper I.....	33
Paper II.....	47
Paper III.....	59

1 Introduction

Thin films[†] are deposited onto a substrate to enhance or add properties to the combined material system. The thickness of the films can range from a few atomic layers to several micrometers. Thin films can be used in a pure decorative purpose as in the case of earliest known use where the Egyptians hammered gold into leaves with a thickness below 1 μm [1]. However, the ability to combine different substrate and thin film materials opens up for opportunity to tailor also other material properties. Today the use of thin films are therefore widely spread in many different areas and used for a large variety of purposes. For example, there are anti-reflective coatings for eyeglasses and hard coatings to increase the wear-resistance of cutting tools.

Coatings are also often used in electrical contact applications. This is done, e.g., to protect the contact from oxidation and to lower the contact resistance. Two well-used materials for contact applications are the noble metals Au and Ag. Au has a good oxidation resistance, but is expensive. Ag is less expensive, but tends to tarnish in the presence of sulfides or chlorides. It is therefore motivated to try to replace these two metals with other coatings.

The focus of my research in this aspect has been at the Ti-Si-C and Nb-(Si)-C systems. The aim of the work is to investigate how the properties and structure change with composition of the chosen material systems. In the case of Ti-Si-C, I try to get a deeper understanding on how Si is incorporated in the NaCl-structure TiC_x phase as well as how Si segregates to form a composite material at low temperatures. This information has been lacking although Ti-C and Ti-Si-C-based nanocomposites have already been investigated for both tribological and electrical applications. In the case of Nb-C, the system was previously only screened and found interesting by Lewin [2] in the aspect of candidate for electrical contact applications. Here, I investigate the system in more detail with respect to microstructure as well as electrical and mechanical properties. I find that it is at least as good as the Ti-C system in electrical contact applications.

Much of the conclusions in the work is related the microstructure as determined by high resolution transmission electron microscopy (TEM). It is therefore important that the TEM investigations are correct and no electron-beam-induced damages, leading to wrong conclusions, occurs. During our TEM observations I found that amorphous Nb-Si-C coatings crystallized due to the electron beam. I therefore try to understand the mechanism behind electron-beam-induced crystallization as well as how this can be avoided. In the investigation we also add

[†] Sometimes the word *coating* is also used in the field. In some contexts this word is used for thin films thicker than $\sim 1 \mu\text{m}$. In other contexts the word coating is used for all deliberately added layers, while films are referring to thin layers of contamination. In this thesis both the terms coating and thin film are used for deliberately deposited layers.

the related Zr-Si-C system to see how the crystallization is related to the choice of transition metal.

References

- [1] M. Ohring, **Materials science of thin films, 2nd ed.**, Academic press, (2002)
- [2] E. Lewin, **Design of Carbide-based Nanocomposite Coatings**, PhD thesis, ISBN: 978-91-554-7636-6, Uppsala, (2009)

2 Electrical contacts

Electrical contacts are of importance for this thesis since my collaboration with the industrial partners in FunMat theme 1 deals with the development of coatings[†] for electrical contact applications. This is reflected in **Paper III**, where we investigate how the microstructure influences electrical properties of Nb-C coatings. The following chapter will give a brief introduction to the function of electric contacts and available contact materials. More detailed description of electrical contact theory can be found e.g. in texts written by Holm [1], Slade [2], and Braunovic [3].

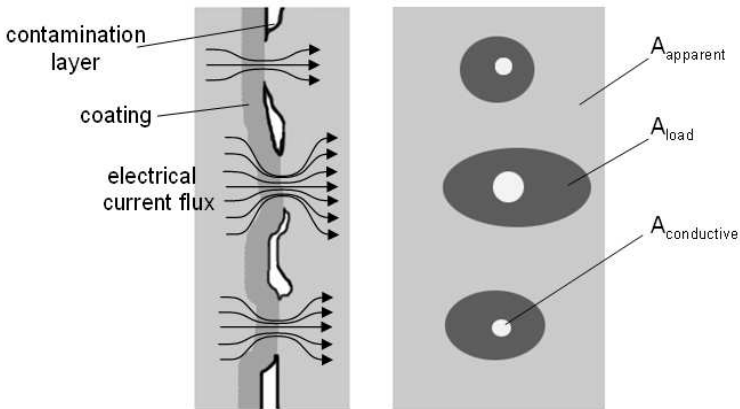


Fig. 2.1 Schematic figure of the cross-section (left) and plan view (right) of an electrical contact. (After Lewin [4])

An electrical contact is according to the definition by Holm [1] “a releasable junction between two conductors which is apt to carry electric current”. I.e. two surfaces (contact members) that when in contact with each other are able to carry electrons from one of the contact members (cathode) to the other contact member (anode). However, the surface interaction between the contact members can be complex. This is illustrated in **Fig. 2.1** which shows schematic figures of an electrical contact in cross-section (left), and plan-view (right). This contact consists of one coated and one uncoated part, which are pressed together by a contact force. Although the apparent contact area, A_{apparent} , may seem large, surface roughness will reduce the actual load bearing area, A_{load} , where an electric current can flow. If the materials also include non-conducting phases, e.g., an insulating oxide on the surface, the actual conductive area, $A_{\text{conductive}}$, will consist only of the small areas where the contact pressure is high enough to break through the oxide. The conducting spots out of which $A_{\text{conductive}}$ consists are called a-spots.

[†] Note that in the field of electrical contacts the terms “film” or “thin film” is often referring to a contamination layer formed on top of the contact. To avoid confusion these terms are not used in this chapter.

At an a-spot the electrical current flux is much higher than in the bulk of the contact. This gives rise to a constriction resistance in the contact. The total constriction depends on the area and distribution of the a-spots. The contact resistance, which is an important property of all electrical contacts, is mainly caused by the constriction resistance. Therefore the contact resistance is not only a property of the contact material, but also of the application (e.g., force applied) and surface contamination.

Electrical contacts are found in all electrical systems. The requirements on these contacts are different depending on in which regime they are supposed to work, e.g., at high or low contact force, and how their mechanism is designed, e.g., sliding or permanent contact. Except for being a good electrical conductor and having a low contact resistance, contact materials also have to be corrosion resistant and ductile. In this thesis possible applications for the investigated material systems, Nb-C and Ti-Si-C, involve non-static contacts. This adds wear resistance and low friction to already mentioned properties.

The electrical and mechanical properties of the top surface are often the most crucial part in electrical contacts. A contaminated surface will increase the contact resistance and reduce performance of the contact. Therefore, contacts are often coated. Not only the functionality of the coating is then of importance, but also the adhesion to the substrate, the cost, and the environmental impact of the deposition must be considered.

The dominant method of producing electrical contact coatings today is by plating. In electroplating metal ions are deposited onto a conductive surface from an electrolytic bath. Electroplating can be used for dense coatings. Another plating method is a chemical reduction process called electroless plating. In the process coating growth will occur on a activated surface immersed in the plating solution. Both methods can be used for complex shapes. However, there are limitations for which materials and compositions that can be used. There is also an environmental issue with dangerous chemicals from the plating bath.

An alternative method that is used for the coatings presented in this thesis is physical vapor deposition, PVD (see **Ch. 4** for a more detailed description of this method). The main advantage over plating is that a much wider range of materials and compositions can be deposited. PVD is also a more flexible technique for changing between different coating materials in the deposition system and is more environmental friendly. One disadvantage is that the method is non-selective, which means that the coating material will be deposited also on, e.g., the chamber walls. This can result in a waste of expensive coating materials.

As substrate material for electrical contact coatings Cu-based alloys are often used, e.g., brass or bronze. Cu is used since it is relatively inexpensive and at the same time have very good electrical and thermal conductivity. The drawback is a relatively low deformation temperature (200-300 °C) [3]. A diffusion barrier of Ni is often used to hinder the Cu from diffusion through the top coating and serve as

load support. The top coating is often a noble metal or alloy in order for the contact resistance to remain low and stable over the lifetime of the contact. An alternative to Cu-based alloys is stainless steel, which is cheaper than Cu and has good corrosion properties.

Among the noble metals, Au has the best resistance against oxidation, but is at the same time a very soft metal. It is therefore a very good contact material for low-current and low contact force applications [5] such as mobile phones and other hand-held electronics. Adding small amounts of Ni and Co increases hardness and wear resistance. These alloys are therefore often called hard gold. The main drawback with Au is the high price and high environmental impact when deposited by electro plating.

A less expensive alternative to Au is Ag. Ag has the lowest electrical resistivity and highest thermal conductivity of all elements. However, if Ag is exposed to sulfides [6] or chlorides [7] it will tarnish and form a contamination layer that will decrease the performance. To protect Ag from tarnish it can be alloyed with Pd [8], but at a much higher production cost of the coating.

The high price of Au and the tarnishing of Ag motivate a search for new materials. In order to allow for tribological improvements and at the same time retain good electrical properties, nanocomposite materials have been investigated. Special interests have been paid to binary and ternary systems of transition metals and carbon, such as Ti-C and Ti-Si-C [9-12]. These systems often consist of metal-carbon grains in a matrix of amorphous C. The properties can be controlled by the structure, e.g., grain size and matrix thickness, as well as the choice of metal [13-15]. Most nanocomposite coatings can be deposited at low temperatures and are therefore useful for industrial substrates such as Cu, which softens already at ~200 °C [3]. Studies to scale up the deposition process to meet industrial demands such as larger deposition areas and higher deposition rates have been successful [9-10].

However, to be able to develop new nanocomposite materials for electrical contact applications a further understanding on how the structure and composition affects the properties is needed. This is as mentioned in the beginning of this chapter done with the Nb-C system in **Paper III**, where we show how the microstructure influences electrical properties.

References

- [1] R. Holm, **Electric Contacts, Theory and Application, 4th ed.**, Springer-Verlag, Berlin, (1967)
- [2] P.G. Slade, ed., **Electrical contacts – Principles and applications**, CRC Press, Taylor & Francis Group, New York, (1999)
- [3] M. Braunovic, **Electrical contacts – Fundamentals, applications and technology**, CRC Press, (2006)
- [4] E. Lewin, **Design of Carbide-based Nanocomposite Coatings**, PhD thesis, ISBN: 978-91-554-7636-6, Uppsala, (2009)

- [5] M. Antler, **Tribology of metal coatings for electrical contacts**, *Thin Solid Films* 84 (1981), 245-256
- [6] J.P. Franey, G.W. Kammlott, T.E. Graedel, **The corrosion of silver by atmospheric sulfurous gases**, *Corrosion Science*, 25 (1985), 133-143
- [7] W. Rieder, **Electrical contacts – An introduction to their physics and applications**, *IEEE, Piscataway, NJ*, (2005)
- [8], M. Doriot-Werlé, O. Banakh, P.-A. Gay, J. Matthey, P.-A. Steinmann, **Tarnishing resistance of silver–palladium thin films**, *Surface & Coatings Technology* 200 (2006) 6696–6701
- [9] E. Lewin, E. Olsson, B. André, T. Joelsson, Å. Öberg, U. Wiklund, H. Ljungcrantz, U. Jansson, **Industrialisation study of nanocomposite nc-TiC/a-C coatings for electrical contact applications**, *Plasma Processes and Polymers* 6 (2009) 928–934
- [10] J. Lauridsen, P. Eklund, T. Joelsson, H. Ljungcrantz, Å. Öberg, E. Lewin, U. Jansson, M. Beckers, H. Högberg, L. Hultman, **High-rate deposition of amorphous and nanocomposite Ti–Si–C multifunctional coatings**, *Surface & Coatings Technology* 205 (2010) 299–305
- [11] Å. Öberg, Å. Kassman, B. André, U. Wiklund, M. Lindquist, E. Lewin, U. Jansson, H. Högberg, T. Joelsson, H. Ljungcrantz, **Conductive nanocomposite ceramics as tribological and electrical contact materials**, *Eur. Phys. J. Appl. Phys.* 49, 22902 (2010)
- [12] P. Eklund, J. Emmerlich, H. Högberg, O. Wilhelmsson, P. Isberg, J. Birch, P.O.Å. Persson, U. Jansson, L. Hultman, **Structural, electrical, and mechanical properties of nc-TiC/a-SiC nanocomposite thin films**, *J. Vac. Sci Technol B*, 23 (2005) 2486-2495
- [13] D. Munteanu et al., **Influence of composition and structural properties in the tribological behaviour of magnetron sputtered Ti–Si–C nanostructured thin films, prepared at low temperature**, *Wear* 268 (2010) 552-557
- [14] M. Andersson, S. Urbonaite, E. Lewin, U. Jansson, **Magnetron sputtering of Zr–Si–C thin films**, *Thin Solid Films* 520 (2012) 6375–6381
- [15] J. E. Krzanowski, J. Wormwood, **Microstructure and mechanical properties of Mo–Si–C and Zr–Si–C thin films: Compositional routes for film densification and hardness enhancement**, *Surface & Coatings Technology* 201 (2006) 2942–2952

3 Material systems

In this thesis the studied materials are carbides based on a transition metal (Me) from either group 4 (Ti and Zr) or group 5 (Nb) in the periodic table. Since the structure of these materials are of great important for the material properties, a short note explaining the different structures observed in this thesis is made. These structures range from *epitaxial* TiC (**Paper I**), through *composites* of Ti-Si-C and Nb-C (**Paper I** and **III**, respectively), to *amorphous* Nb-Si-C and Zr-Si-C (**Paper II**).

An epitaxial material is a single crystal material grown with a relationship to the substrate. The epitaxy can, e.g., be analyzed using pole figures (**Ch.** 5.2.2) or electron diffraction (**Ch.** 5.1.1) and is described by indicating one common plane (()-brackets) and one common direction ([]-brackets) for the film and substrate. In the case of TiC on Al₂O₃(0001) this means with TiC(111)//Al₂O₃(0001) and TiC[011]//Al₂O₃[1100] or TiC[011]//Al₂O₃[1100] depending on the stacking sequence of TiC(111). This means that the TiC film will consist of two domains rotated 180° with respect to each other and with common (111) planes parallel to the surface.

The word composite means that the material consists of at least two phases. Each phase can be either amorphous or crystalline and consist of one or more elements. For example in the case of the Nb-C system in **Paper III**, crystalline NbC grains are embedded in a matrix of amorphous C. This is often written as c-NbC/a-C. To emphasize that the size of the crystalline NbC grains are smaller than 100 nm in one or more dimensions (i.e. are nano-crystalline [1]) “nc-“ can be added to NbC so it now reads nc-NbC/a-C. In the same way a system can also be called a *nanocomposite* when one or more of the phases in the composites are restricted to a size less than 100 nm in at least one dimension.

The definition for an amorphous material is often unclear. With X-ray amorphous we address a material, which does not give any or very broad peaks in X-ray diffraction measurements. However, these materials can still contain crystalline grains of the order of a few nanometers. Even when viewed in high resolution TEM there can be a problem to distinguish between amorphous and nanocrystalline materials since also amorphous materials can have a short-range order. [2] In **Paper II I** consider materials with crystalline particles larger than ~1.5 nm to be nanocrystalline.

3.1 Me-C

The metal carbides studied in this thesis belong to the refractory carbides. They all share properties such as high hardness and high melting point together with semimetallic electrical conductivity. [3] One other common factor is that they form NaCl (B1) structures with C at the interstitial octrahedral sites of the Me fcc lattice. For Ti and Zr, this is the only carbide phase while for Nb there also exists

an $\text{Nb}_2\text{C}^\dagger$ phase [5]. The B1 phases are non-stoichiometric and therefore often written as MeC_x , where x is the carbon to metal ratio. The stability range is wide with $0.50 < x < 0.97$ [5], $0.72 < x < 1.0$ [5], and $0.61 < x < 1.0$ [6], for Ti, Nb, and Zr, respectively. The carbon content has a large influence on the lattice parameter [4], which changes parabolically. The smallest value for the lattice parameter is found at the lowest value of x in the stability range. For the Zr and Ti carbides the maximum value is, however, not at maximum x .

With increasing carbon content the excess of C starts to form an amorphous phase turning the MeC system into a two-phase system of nc-MeC/a-C. Even higher carbon content reduces the grain size further and the amount of a-C matrix increases. Not only the structure, but also mechanical and electrical properties change with the C content. This can be seen in **Paper III**, where changes in hardness, elastic modulus, resistivity, and contact resistance are presented as a function of C content.

3.2 Me-Si-C

When Si is added it will affect both the structure and the properties of the material. For example, Si disturbs the growth of MeC crystal grains and therefore reduces the grain size.

For deposition of Ti-Si-C at high temperatures (above ~ 700 °C), the Ti_3SiC_2 MAX phase can form [7]. Because of heat sensitive substrates (e.g. Cu) we are however, more interested in lower deposition temperatures (< 400 °C) where the Ti-Si-C instead tends to form in a nanocomposite structure with TiC grains embedded in a matrix of SiC. This is a well-studied system, which combines high hardness and low friction [8-9] with good electrical properties [10-11]. Understanding of how the Si interacts with the TiC and segregates to form a composite material is an important key to be able to explain these properties. In **Paper I** we therefore use a simplified model system of epitaxial TiC_x ($x \sim 0.7$) to investigate how low contents of Si is gradually incorporated in the structure.

At a Si content of ~ 20 - 30 at.% these Me-Si-C structures becomes amorphous [12-14]. In order to verify the transition of the system from nano-crystalline to amorphous, electron microscopy with high spatial resolution is preferred. However, the energetic electron irradiation during TEM studies can obstruct the interpretation of the micrographs. In **Paper II** we show how to avoid this problem.

[†] This phase has a narrow range of existence at low temperatures [4], and probably due to the high carbon content in our films, it was never observed in this thesis.

References

- [1] S.C. Tjong, H. Chen, **Nanocrystalline materials and coatings**, *Materials Science and Engineering R* 45 (2004) 1–88
- [2] A. Cavaleiro, J.Th.M De Hosson, **Nanostructured Coatings**, Springer, (2006)
- [3] W.S. Williams, **Physics of transition metal carbides**, *Materials Science and Engineering*, A105/106 (1988) 1-10
- [4] E.K. Storms, **The refractory carbides**, Academic Press, (1967)
- [5] L.E. Toth, **Transition metal carbides and nitrides**, Academic Press, (1971)
- [6] H. Okamoto, **C-Zr (Carbon-Zirconium)**, *Journal of Phase Equilibria* 17 (1996) 162
- [7] P. Eklund, M. Beckers, U. Jansson, H. Högberg, H. Hultman, **The Mn+1AX_n phases: Materials science and thin-film processing**, *Thin Solid Films* 518 (2010) 1851-1878
- [8] T. Zehnder, J. Matthey, P. Schwaller, A. Klein, P.-A. Steinmann, J. Patscheider, **Wear protective coatings consisting of TiC–SiC–a-C:H deposited by magnetron sputtering**, *Surface and Coatings Technology* 163–164 (2003) 238–244
- [9] D. Munteanu et al., **Influence of composition and structural properties in the tribological behaviour of magnetron sputtered Ti–Si–C nanostructured thin films, prepared at low temperature**, *Wear* 268 (2010) 552-557
- [10] J. Lauridsen, P. Eklund, T. Joelsson, H. Ljungcrantz, Å. Öberg, E. Lewin, U. Jansson, M. Beckers, H. Högberg, L. Hultman, **High-rate deposition of amorphous and nanocomposite Ti–Si–C multifunctional coatings**, *Surface & Coatings Technology* 205 (2010) 299–305
- [11] P. Eklund, J. Emmerlich, H. Högberg, O. Wilhelmsson, P. Isberg, J. Birch, P.O.Å. Persson, U. Jansson, L. Hultman, **Structural, electrical, and mechanical properties of nc-TiC/a-SiC nanocomposite thin films**, *J. Vac. Sci Technol B*, 23 (2005) 2486-2495
- [12] M. Andersson, S. Urbonaite, E. Lewin, U. Jansson, **Magnetron sputtering of Zr–Si–C thin films**, *Thin Solid Films* 520 (2012) 6375–6381
- [13] M Naka, H. Sakai, M. Maeda, H. Mori, **Formation and thermal stability of amorphous Ti-Si-C alloys**, *Mat. Sci. Engin. A* 226, (1997) 774-778
- [14] N. Nedfors, O. Tengstrand, P. Eklund, L. Hultman, U. Jansson, **Multifunctional amorphous and nanocomposite Nb-Si-C coatings deposited by DC magnetron sputtering**, *In manuscript*

4 Deposition process

There are several techniques for deposition of thin films. Wet chemical processes such as *electroplating* uses an electrolyte to transport metal ions and deposits them on a conducting surface. In *vapor deposition* the material is transported to the substrate in a gas phase. Vapor deposition can be further divided into the categories of *chemical vapor deposition* (CVD) and *physical vapor deposition* (PVD). In CVD the film growth occurs through chemical reactions introduced by the precursors in gas phase. This method is useful for complex substrate surfaces since the gas can go into cavities. However, the reactions in CVD often require high temperatures, which limit the choices of substrates. For heat-sensitive substrates PVD can instead be used. One common way of vaporizing the material in PVD is by *sputtering* where atoms in the source material are hit by ions and ejected towards the substrate [1]. The use of sputtering was reported by Grove as early as 1852 [2]. Sputtering or more precisely a variant called *dc magnetron sputtering* is also the technique used for all the films analyzed in thesis and therefore *magnetron sputtering* will be described more in detail in the following section.

4.1 Magnetron sputtering

Fig. 4.1 shows a schematic figure of the magnetron sputtering process. In the process atoms are ejected from the source (target) by ions from the plasma. The atoms then travel through the chamber (and the plasma) and some of them end up at the substrate where they can be deposited. To avoid contamination from other elements in the film, magnetron sputtering is performed at low background pressure in a vacuum chamber. A gas is introduced to the chamber to provide the ions that ejects the target-atoms. If no reactions with the gas are wanted (non-reactive sputtering) an inert gas, typically Ar (as for the films in this thesis), is used. Otherwise e.g. oxides and nitrides can be deposited by the use of O_2 and N_2 as gas, respectively. The ions are formed in a plasma[†], which is ignited when free electrons (available in the chamber due to, e.g., cosmic radiation or thermal energy) are accelerated by an applied electric field and undergoes inelastic collisions with neutral gas atoms.

At the target, a negative potential is used to attract and accelerate the ions in the plasma. When the ion hits the target several events can occur. Some of them are illustrated in the left part of **Fig 4.1**. Firstly, secondary electrons and photons can be emitted. The secondary electrons are important because they ionize atoms in the plasma and in this way the plasma can be sustained. The ions, in turn can knock out (sputter) atoms from the target, either directly or via a cascade of collisions. How many atoms that are sputtered per incident ion is called sputter

[†] Although we here mainly talk about the plasma ions, the plasma in itself is a quasi-neutral gas. This means that it consists of electrons, ions and neutrals without any net-charge. [3]

yield and is dependent on the sputtered material and the energy of the impinging ions.

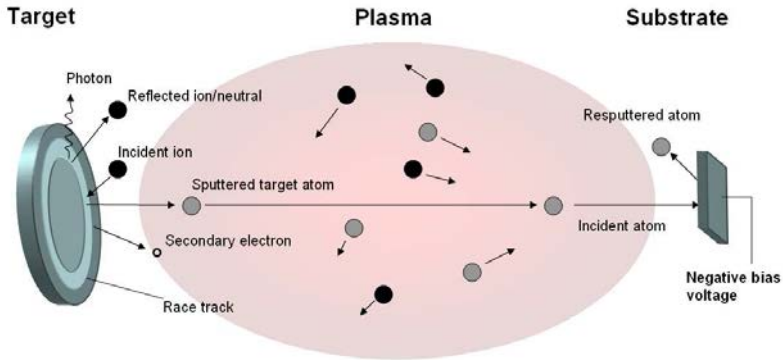


Fig. 4.1 Schematic figure of the sputtering process. Atoms from the target are transported through the plasma and deposited on the substrate.

In order to increase the degree of ionization close to the target where the ions are needed for the sputtering process, magnets are put behind the target (hence the name *magnetron* sputtering). The formed magnetic field will trap the secondary electrons and thus confine the space where most of the ions are created. The confinement of the electrons will cause an uneven sputter rate over the surface of the target where most of the sputtered atoms come from the so called *race track*. However, too much confinement of the plasma near the target can be undesirable since plasma ions also modify the growth conditions at the substrate. This problem can be solved by an unbalanced magnetron, in which the magnetic field is strengthened at the inner or outer parts of the target. Thereby more of the secondary electrons can escape from their confinement and ionize atoms further away from the target.

The sputtered atoms will travel in the direction they are ejected until they reach the chamber wall, the substrate or collide with another atom (or ion). In such collisions, the atoms will change direction. If collisions occurs often enough the motion of the atoms will become random. These atoms are called thermalized. The average distance an atom can travel before a collision is called the *mean free path*, λ [4]. At an Ar pressure of 0.4-0.5 Pa, which is used as working pressure for the sputter depositions in this thesis, λ is roughly a couple of centimeters with longer mean free paths for the lighter elements.

An atom that lands on the substrate surface it is called adatom. The *sticking coefficient* is the probability that the atom will stay on the surface. If the adatom has some energy it can move around on the surface. The adatom mobility can be manipulated with bombardment of energetic particles. This can be achieved by applying a negative bias voltage, which attracts the ions in the plasma. The ion bombardment can increase the nucleation rate and the film density, but also the

stress state in the film [5]. If too high bias is applied to the substrate, the plasma ions will start to resputter the material of the substrate.

With magnetron sputtering it is possible to deposit a wide range of materials from metals to insulators. For deposition of thin films consisting of more than one element, composite targets are available and these are often used in industrial processes where the wanted composition is known. However, when investigating how different compositions cause structural changes like in **Paper I and III**, the use of several elemental targets will give a larger possibility to control the composition. Elemental targets were therefore used for the deposition of all films in this thesis.

The text above describes how the sputtering is caused by ions accelerated by a negative potential. There are several different techniques to do this. For the films in this thesis a constant voltage was applied (*dc magnetron sputtering*). This technique can not be used for target materials with a resistivity larger than $10^6 \Omega\text{cm}$. [1] For these material, an ac or radio frequency (rf) voltage need to be applied (*ac or rf magnetron sputtering*). The high frequency will lower the impedance of the material and allow a current to pass. Since the electrons follow the changes in the electric field much faster than the ions, the target will become self-biased to a negative potential. In this way the sputtering process can go on in the same way as for a DC target with positive ions that sputter away target atoms. *Pulsed magnetron sputtering* can be used if arcing is a problem in the system. By inverting the voltage in a pulse the electrons in the plasma can discharge the target to prevent large charges from building up.

References

- [1] M. Ohring, **Materials science of thin films**, 2nd ed., Academic press, (2002)
- [2] P. M. Martinn, **Handbook of deposition technologies for films and coatings: science, applications and technology**, 3rd ed., Elsevier Science, (2010)
- [3] F.F. Chen, **Introduction to plasma physics and controlled fusion- Volume 1: Plasma physics**, 2nd ed., Plenum Press, (1984)
- [4] J.F. O'Hanlon, **A user's guide to vacuum technology**, 3rd ed., John Wiley & Sons, (2003)
- [5] I. Petrov, L. Hultman, J.E. Greene, **Microstructural evolution during film growth**, *J. Vac. Sci. Technol. A* 21(5) (2003) 117-128

5 Characterization

A large number of techniques are used to analyze the structure and properties of thin films. In this chapter some of the techniques used in this thesis will be described. The first is *transmission electron microscopy*, integrated with *energy-dispersive X-ray spectroscopy* (EDX). TEM/EDX is used in **Paper I-III** to observe the structure and elemental distribution of the materials. Next, different methods using *X-ray diffraction* are discussed. These methods include θ - 2θ (**Paper I**) and *grazing incident* (**Paper III**) *X-ray diffraction* which are used for determining the crystalline phases in the materials. They also includes *pole figures* and the *sin² ψ -method* (**Paper I**), which are used to determine the epitaxy and strain-free lattice parameter, respectively. The last method described is *X-ray photoelectron spectroscopy* (XPS), which is used to determine the composition (**Paper I-III**) and describe the bonds between the atoms (**Paper I and III**).

5.1 Transmission electron microscopy (TEM)

One of the more important techniques considering the work in this thesis is the transmission electron microscopy. It is a powerful technique since it combines high spatial resolution with crystal information from electron diffraction. In **Paper I and III** it is used to help determine the structural evolution of the studied materials on the nano-scale. TEM can also be combined with other analytic methods to get information about the distribution and composition of the elements in the film. One example is EDX, which is used in **Paper I** in order to show segregation of Si. In the TEM electrons are emitted from an electron gun and accelerated by a high voltage. (In work related to this thesis, typically ~200 kV). An advanced set-up of magnetic lenses is then used to focus and direct the beam through the microscope and form an image of the sample. In this chapter focus will be on how an image or diffraction pattern is formed and used after a beam with parallel electrons has hit the sample. Some time will also be spent on EDX and sample preparation. The problem with electron-beam-induced damage (**Paper II**) will be presented in **Ch. 6**.

5.1.1 Imaging

Since the wavelength of the electrons at 200 keV are very small (2.5 pm), the theoretical resolution of the microscope is as high as 0.02 Å. In practice due to instrumental and atomic aberrations the best spatial resolution is not that high, but is still enough for atomic resolution.

Fig. 5.1 shows a simplified model of the electron path through the sample and down to a fluorescent screen or CCD-camera. In a) the imaging system is shown. It consists of three lenses. The *objective lens* forms the first image of the sample. The corrections of this lens are important since all imaging errors made by the lens will be magnified by the other lenses in the system. The second lens is called the *intermediate lens*. By changing the lens current (pressing a button) for the intermediate lens the operator can switch between diffraction and imaging. The

last lens, *the projector lens*, magnifies the image or diffraction pattern of the sample even further.

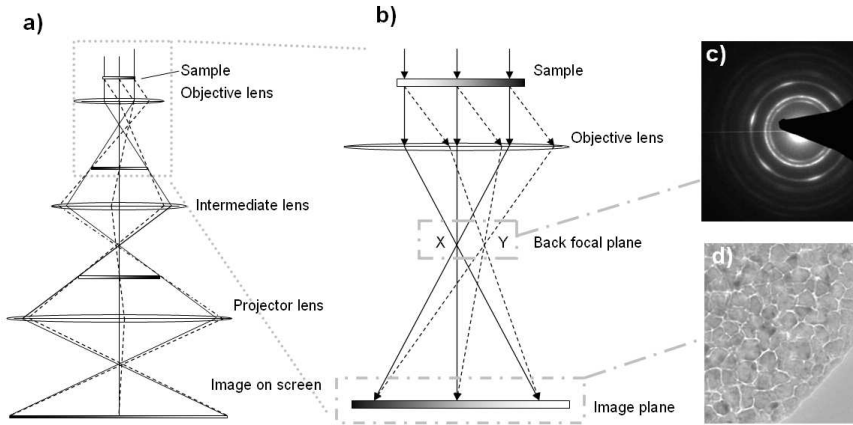


Fig. 5.1 a) simplified model of the electron path through the imaging lenses, b) projection of the image in the objective lens, c) selected area electron diffraction and d) real space micrograph.

Fig. 5.1b) shows the projection in the objective lens. As the electrons go through the sample they can interact with material in several different ways. Some of them are transmitted without any change (solid lines), while others are scattered by the atoms in the sample (dashed lines). All the electrons scattered in one direction will come together in a point in the back focal plane. (I.e. point X for the direct beam and point Y for the scattered electrons in the figure.) All the points together make up the electron diffraction pattern. The electron path can thereafter be further extended to the image plane where an image of the sample is formed.

An example of an electron diffraction pattern (Ti-Si-C sample, **Paper I**) is shown in **Fig. 5.1c)**. The image of the diffraction pattern is formed by putting the object plane of the intermediate lens in the back focal plane of the objective lens. The pattern in the figure consists of circles which are more intense in some of the areas. The black triangular shape is a beam blocker, which is used to protect the CCD-camera from the high intensity of the directly transmitted beam. From the pattern we can obtain information about the lattice spacings (radii of the circles), crystal structure (distribution of the circles), and crystal orientation. A circle with homogenous intensity indicates a poly-crystalline structure with unordered crystallites. In the viewed sample there is, however, some ordering (a (111) preferred direction) among the crystallites and therefore the third circle from the center has higher intensity in some directions (the {220} spots). In this way more and more order will finally give rise to a dot pattern when the intensities from the rings are concentrated in specific directions or vanish depending on the orientation of the grains. Amorphous material (studied in **Paper II**) will scatter equally in all directions and therefore only form very diffuse circles. There is often a wish to have diffraction patterns from only one part of the prepared sample (e.g., excluding the substrate). This can be done by inserting an aperture (*selected area*

aperture) in the image plane of the objective lens. The area of the image where the beam then can pass is the same as from which the viewed diffraction pattern originates.

The real space image corresponding to **Fig. 5.1c**) is shown in **Fig. 5.1d**). The image is formed by putting the object plane of the intermediate lens in the image plane of the objective lens. The scattered electrons are important for imaging since they make up most of the image contrast. The image contrast can be increased by inserting an aperture (*objective area aperture*) in the back focal plane of the objective lens. If the electrons in point Y (**Fig. 5.1b**)) are blocked, regions scattering more in this direction will appear darker since these electrons do not contribute to the image anymore. If the transmitted beam (point X) is screened by the objective aperture, all the image contrast is made up of scattered electrons. All regions not scattering electrons (e.g., a hole in the sample) will appear totally black and this technique is therefore called dark field imaging. The technique can be useful for identifying crystal grains with a certain orientation, by selecting this orientation with the objective area aperture in the diffraction mode. These grains will then appear bright in imaging.

Thus, atomic resolution together with the ability to easily record diffraction patterns is one of the big advantages of TEM since it is possible to obtain both real and reciprocal space information from a specifically selected part of the sample. The microscope can also be equipped with other instruments such as EDX (see **Ch. 5.1.1.2**) or EELS to be able to obtain compositional information.

However there are also some drawbacks with TEM. One disadvantage is that the sample has to be electron transparent (i.e. <100 nm for most materials). This means an extensive sample preparation (See **Ch. 5.1.3**) which in worst case might affect the composition. The sample preparation usually gives only a very small volume from each sample that can be imaged. The investigated volume then has to be assumed representative for the whole film. Care should also be taken not to misinterpret features, e.g., overlapping grains when the 3-dimensional volume of the sample is projected into a 2-dimensional image.

5.1.2 Energy-dispersive X-ray Spectroscopy (EDX)

As earlier mentioned TEM can be implemented together with other instruments. In EDX (also called EDS) the energy of emitted X-rays from the sample are analyzed. This is possible because atomic electrons in the sample can be excited by the beam. After the excitation an electron from a shell further out will take the excited electrons place in order to lower the energy of the atom and at the same time an X-ray photon is emitted. The energies (wave-lengths) of the emitted photons are characteristic for each element and can therefore be used to identify the elements. [1] As an example, the EDX spectrum from a Ti-Si-C sample is shown in **Fig. 5.2**. In the spectra the peaks of the materials in the film is clearly seen.[†] The intensity

[†] In addition also a small Al peak just below the Si peak can be seen. This peak probably originates from material coming from the Al₂O₃ substrate.

of the different peaks depends on composition, but also on the type element. Sensitivity factors can be used in quantitative analysis, but care should be taken especially for the lighter elements (in this case C), which are hard to quantify. EDX are therefore a qualitative rather than quantitative method.

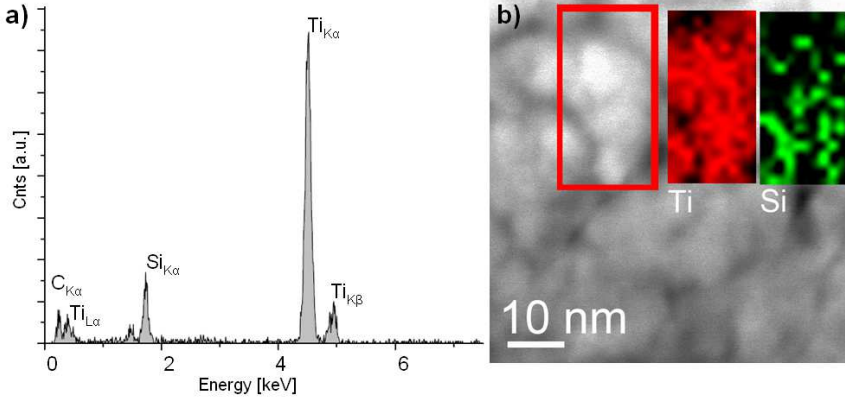


Fig. 5.2 a) example of EDX spectrum from a Ti-Si-C sample. b) STEM micrograph from the same Ti-Si-C sample with EDX map of Ti and Si from the marked region inserted.

A special variant of TEM often used in connection with EDX is *scanning transmission electron microscopy* (STEM). In STEM the beam is focused to a small spot and the image is formed by continuous scanning over an area. The advantage of this is that an EDX spectrum can be acquired from a very small region. The use is shown in **Fig. 5.2b**) where elemental mapping of Si and Ti (insets) have been performed. The maps are created by requiring one EDX spectrum for each point in the marked region. In each spectrum the intensity of the Ti_{Kα} and Si_{Kα} peak is integrated and plotted in the Ti and Si map, respectively. This example comes from **Paper I**, and shows us how Si has segregated from the TiC structure out to the grain boundaries.

5.1.3 Sample preparation

There are several ways to prepare electron transparent specimens. Most of the TEM images presented in this thesis are from cross-sectional specimens. This means that the film has to be cut and glued into a grid with two film sides facing each other. The specimens are then mechanically polished down to a thickness of $\sim 50 \mu\text{m}$ and a surface roughness of $\sim 1 \mu\text{m}$ before they are put in an ion miller. In the ion miller the specimens are thinned further by Ar⁺ ions with energy of 5 keV to achieve electron transparency. In a final step the energy of the Ar⁺ ions are reduced to 2 keV for 10 min in order to remove residuals from the surface.

An important aspect is how the sample preparation affects the structure and chemical composition of the material. It is for example shown that the clean-sputtering with Ar⁺ ions prior XPS measurements changes the binding structure of metastable Ti-Me-C (Me=Al, Fe, Cu or Pt) already at low ion energies (<4 keV). [2] This is in the same range as the Ar⁺ energy used for the ion milling in TEM

sample preparation and the question of ion induced damage in the samples are thus motivated. In **Paper II** we therefore compare Nb-Si-C TEM specimens prepared by ion milling, and specimens prepared by the *small angle cleavage technique* (SACT) [3]. In SACT the sample is cleaved in such way that electron transparent regions are formed. Therefore, no ion milling is necessary for this method. However, often only a very small region will be electron transparent [4]. In the case of Nb-Si-C only modest differences were seen between the two methods and the conclusion was that the ion milling did not have any distinguishable effect on these samples.

5.2 X-ray diffraction (XRD)

XRD is well used in material science since it is both easy to use and nondestructive. In XRD, X-rays are radiated onto a material. The X-rays will interact with the material and information about the crystal structure can be obtained from the diffracted X-rays.

5.2.1 Bragg's law

The reason to use X-rays is that their small wavelength, λ , (1.54 Å for $\text{Cu}_{K\alpha}$) is comparable to the distance between the atoms in materials. (I.e., X-rays can resolve the atomic plane spacing.) The X-rays diffract with constructive interference according to Bragg's law

$$n\lambda = 2d_{hkl}\sin(\theta) \quad (5.1)$$

where n is an integer, d_{hkl} the plane distance between two planes with index hkl , and θ the scattering angle. Not all combinations of hkl will give a reflection peak. The allowed reflections are given by the structure factor, which can be calculated from the crystal structure. [5] The peaks positions are dependent on which atoms are present in the structure. Thereby each material will have its own "fingerprint" from which it can be identified using XRD.

The X-ray peaks can only be detected if the condition in **Eq. 5.1** is fulfilled, which implies that the material is crystalline with large enough grains. If the grain size is reduced this is observed as a drop in peak intensity and a peak broadening can also be seen when. The peak broadening can be used to calculate the grain size by using e.g., the "Sherrer's formula" [6]. This is done for the Nb-C samples in **Paper III**. When the grain size becomes smaller than 2-5 nm it is no longer possible to see any reflections and the material is therefore called X-ray amorphous.

5.2.2 Examples of different methods in X-ray diffraction

In order to find the planes that fulfill Bragg's law and in which direction they are oriented, both the incident X-rays and detector as well as the sample orientation need to be varied. The notations of the varied angles in this thesis are illustrated in **Fig. 5.3**.

Several different methods to vary these angles in order to find constructive interference are available. The three of them used in this thesis are illustrated in **Fig. 5.4**. These are a) θ - 2θ , b) *grazing incidence X-ray diffraction (GIXRD)*, and c) *pole figures*. In the figures an epitaxial (A) and a poly-crystalline (B) film of Ti-Si-C are shown.

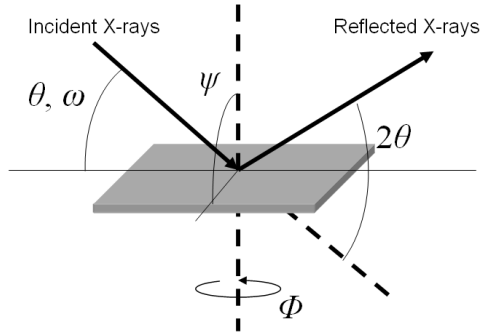


Fig. 5.3 Notation of angles used in XRD.

In a θ - 2θ measurement (illustrated by **Fig. 5.4a**) the incident and reflected angle are changed simultaneously and always kept the same. This means that only crystal planes parallel to the surface will contribute to the diffraction pattern. Film A, which have all the (111) planes oriented this way, therefore show much stronger peaks than B in which the planes are more randomly oriented and the crystallites are smaller.

GIXRD (**Fig. 5.4b**) instead uses an incident beam at a small constant angle, ω , and varies the outgoing angle, 2θ . This means that the planes fulfilling the Bragg's diffraction condition in general are not parallel to the surface. GIXRD is therefore useful when having non-textured materials with grains randomly oriented like film B. For the substrate and film A, the Bragg condition is never fulfilled and therefore no peaks can be seen.

In a pole figure (**Fig. 5.4c**) the outgoing beam and the detector are fixed at one chosen θ - 2θ value, i.e. at one specific plane distance. The sample is then rotated in the ψ and Φ directions and the detected intensity can be plotted onto a stereographic projection. If the sample is highly textured, as for A, the Bragg's condition will only be fulfilled in certain directions and peaks will be seen in the pole figure. If we instead have a less textured sample with grains more randomly distributed in the film the pole intensity will decrease, as for B. In **Fig. 5.4c** the θ - 2θ value was set to correspond to d_{200} for TiC. This value coincides with the d_{0006} value of the $\text{Al}_2\text{O}_3(0001)$ substrate peak and therefore an intense peak can be seen at the center of both pole figures.

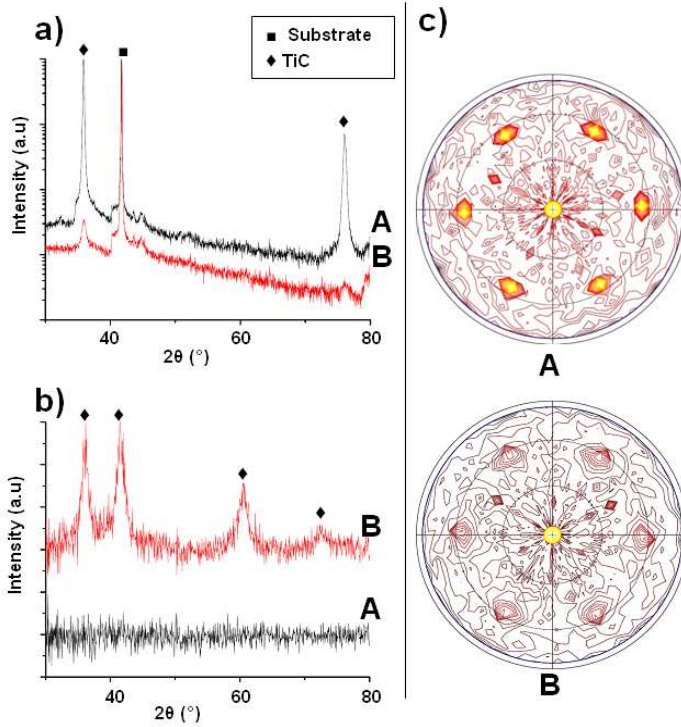


Fig. 5.4 Epitaxial TiC_x (A) and poly-crystalline $Ti-Si-C$ (B), viewed with different X-ray techniques. a) θ - 2θ , b) GIXRD, and c) pole figure of TiC 200.

5.2.3 Strain measurements ($\sin^2\psi$ -method)

In **Paper I** a shift of the (111)-peak was seen with increasing Si content. In order to exclude the possibility that this shift was due to strain the $\sin^2\psi$ -method was used. The accuracy of this method should not be overestimated, but the technique gives an estimate of the in-plane stress, σ and allows for calculation of the strain free lattice parameter a_0 . [7]

A tensile stress in a thin film will cause an expansion of the lattice planes in the direction normal to the surface. At the same time a compression will be seen of the planes parallel to the surface. The expansion and compression is coupled by the Poisson ratio, ν . In the $\sin^2\psi$ -method this change is often observed by measuring the plane distance for a certain plain, d_{hkl} , at different ψ . However, if the stress (as in the case of **Paper I**) is measured on an epitaxial film different d_{hkl} must be chosen for different directions of ψ . In this case the lattice parameter a , rather than a selected plane spacing is used in the plot against $\sin^2\psi$.

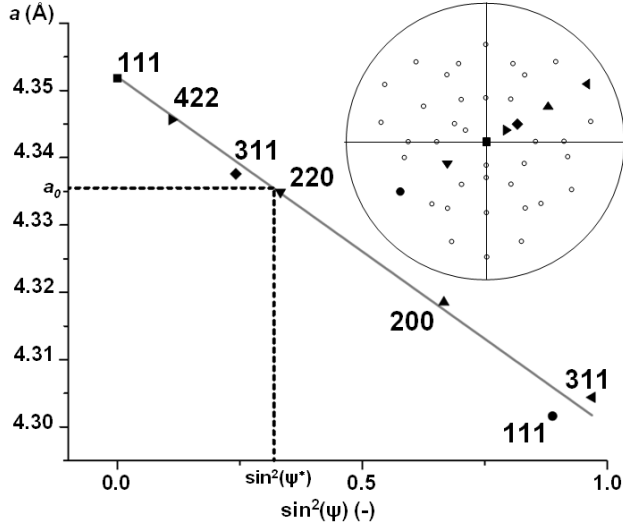


Fig. 5.5 Measurements of the lattice parameter vs. $\sin^2\psi$, and stereographic projection with the measured crystal-directions (filled symbols).

One example of a stress measurement is shown in **Fig. 5.5**. The data points are marked with the indexes of the d_{hkl} from which a was calculated. The positions of the poles are marked with the symbols from plot, in the stereographic projection (inset **Fig. 5.5**). The open circles in the inset show other directions from which a can be measured in the crystal. The figure shows that a linear curve (solid line) can be fitted to the data points. The curve has the equation,

$$a = m \sin^2 \psi + k \quad (5.2)$$

where m and k are constants.

For a stress independent of the azimuth angle Φ , the following equation can be derived (For a more detailed derivation see e.g. [7])

$$\varepsilon = \frac{1+\nu}{E} \sigma \sin^2 \psi - \frac{2\nu}{E} \sigma \quad (5.3)$$

Also knowing that the stress can be expressed as the relative change in a from the strain free lattice parameter it is possible to combine **Eq. 5.2** and 5.3.

$$\frac{1+\nu}{E} \sigma \sin^2 \psi - \frac{2\nu}{E} \sigma = \varepsilon = \frac{a - a_0}{a_0} = \frac{m}{a_0} \sin^2 \psi - \frac{k - a_0}{a_0} \quad (5.4)$$

Identifying the term in front of the $\sin^2\psi$ term gives the stress

$$\frac{1+\nu}{E} \sigma = \frac{m}{a_0} \Leftrightarrow \sigma = \frac{mE}{(1+\nu)a_0} \quad (5.5)$$

If a_0 is not known this can be calculated from the **Eq. 5.2** by first putting $\varepsilon=0$ in **Eq. 5.3**, which gives a value for the strain-free direction ψ^* .

$$\varepsilon = 0 \Rightarrow 0 = \frac{1+\nu}{E} \sigma \sin^2 \psi^* - \frac{2\nu}{E} \sigma \Leftrightarrow \sin^2 \psi^* = \frac{2\nu}{1+\nu} \quad (5.6)$$

The value for $\sin^2\psi^*$ can then be used in Eq. 5.2 to calculate a_0 . From the equations it is clear that the $\sin^2\psi$ -method assumes that the Poisson ratio for the material is known. In the example in Fig. 5.5, the value 0.19 [8] (TiC) is used which gives $\sin^2\psi^*=0.32$. Both $\sin^2\psi^*$ and the corresponding a_0 have been marked in the figure.

5.3 X-ray photoelectron spectroscopy (XPS)

In XPS or ESCA (*Electron Spectroscopy for Chemical Analysis*) X-ray photons are used to eject electrons from the core levels of the analyzed material. Since both the photon energy (E_p) and the work function (W) are known the detected kinetic energy of the emitted electrons (E_k) can be used to calculate the binding energy (E_b).

$$E_b = E_p - E_k - W \quad (5.7)$$

The binding energy is characteristic for each material and by plotting E_b against the intensity a qualitative analysis of the composition can be done. For a quantitative analysis the area of each peak must be calibrated using elemental specific sensitivity factors.

The orbital from which the electrons are emitted will be affected by neighboring atoms. This is seen as a small chemical shift of the peak and thereby different bonds in the material can be detected.

Even if the X-rays penetrate deep into the material, the escape depth of the photoelectrons is usually less than 10 nm which makes XPS a surface sensitive method. For analysis deeper down into the material, sputtering is often used to remove the top surface.

References

- [1] R. Brydson, **Aberration-corrected analytical transmission electron microscopy**, John Wiley & Sons, (2011)
- [2] E. Lewin, M. Gorgoi, F. Schäfers, S. Svensson, U. Jansson, **Influence of sputter damage on the XPS analysis of metastable nanocomposite coatings**, *Surface & Coatings Technology* 204 (2009) 455-462
- [3] S.D. Walk, J.P. McCaffrey, **The small angle cleavage technique applied to coatings and thin films**, *Thin Solid Films* 308-309 (1997) 399-405
- [4] J.P. McCaffrey, **Small-angle cleavage of semiconductors for transmission electron microscopy**, *Ultramicroscopy* 38 (1991) 149-157
- glasses: Atomic structure, crystallization mechanism and stability of an amorphous phase under irradiation**, *Journal of Non-Crystalline Solids* 358 (2012) 502-518
- [5] C. Kittel, **Introduction to solid state physics 8th ed.**, John Wiley & Sons, (2005)
- [6] B.D. Cullity, **Elements of X-ray diffraction**, Addison-Wesley (1956)
- [7] M. Birkholz, **Thin film analysis by X-ray scattering**, John Wiley & Sons, (2009)
- [8] W.G. Sloof, R. Delhez, Th.H. de Keijser, E.J. Mittemeijer, **Development and partial relaxation of internal stresses in thin TiC layers chemically vapour deposited on Fe-C substrates** *J. Mater. Sci.* 22 (1987), 1701-1706

6 Electron radiation damages in TEM

There are several ways in which electron radiation can cause structural and chemical changes to the sample [1-3]. In **Paper II** electron radiation effects on Me-Si-C (Me= Nb or Zr) are investigated. In both cases crystallization of the amorphous phase in the material was found to occur. In order to investigate the cause of the crystallization the following radiation effects were considered.

6.1 Damages caused by elastically scattered electrons

The elastic scattering process can cause damage to the sample by a “knock-on” process between a nucleus in the sample material and the incident electron. The amount of energy that can be transferred (E_T) will be dependent on the incident angle of the electron, the atomic mass and the energy of the electron. **Fig. 6.1** shows the maximum value for E_T when an electron is hitting the nucleus straight on and then backscatters. As can be seen more energy is transferred for light elements and for higher incident electron energies. If E_T is larger than the displacement energy E_d , the atom will be moved from its position as shown in **Fig. 6.2**. If this happens in a crystal (**Fig. 6.2a**) a Frenkel defect consisting of a vacancy and an interstitial can be created. For a high defect density, the material may undergo amorphization. In an amorphous phase (**Fig. 6.2b**), atomic displacement can cause density fluctuation in form of a free volume and an anti free volume. These density fluctuations may in turn crystallize the material [4].

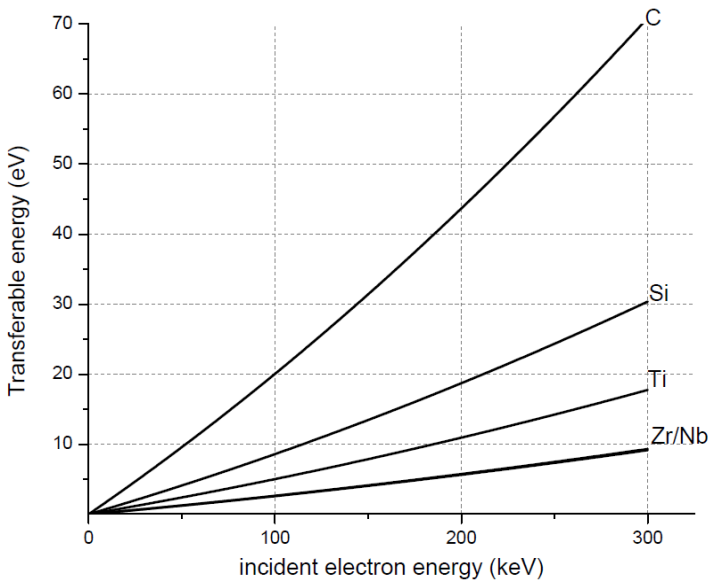


Fig. 6.1 The maximum transferable energy for materials used in this thesis as a function of the energy of the electrons in the electron beam. (The energies are calculated using Eq. 2 in [3])

If the atom hit by the electron is positioned at the surface of the material, the atom can leave the material instead of being displaced. This process is called electron sputtering and the required energy E_s is usually much lower than E_d . Since the electron hitting the atom will be traveling through the sample, sputtering is more likely to occur on the back-side of the specimen.

Table 6.1 shows the values of for the maximum transferable energy to the discussed elements using incident beam electrons with the energy of 200 keV. Shown are also the displacement and sputter energies for some of the elements in their pure form. It should be noted that E_d and E_s are not valid for the investigated materials in the systems since there environment is different compared to there pure states, but should instead be seen as a probable estimate.

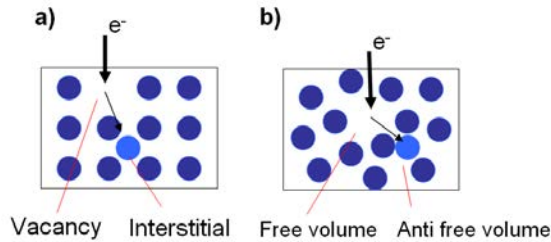


Fig. 6.2 Displacement of atoms may lead to a) creation of Frenkel defects in a crystal, b) density fluctuations in amorphous materials. (Figure reproduced from [5].)

Element	E_T [eV]	E_d [eV]	E_s [eV]
Ti	10.9 ^b	15 ^a	4-8 ^a
Nb	5.64 ^b	24 ^a	6-12 ^a
C	43.7 ^b		
Si	18.7 ^b		
Zr	5.74 ^b		

Table 6.1 Some data for the pure elements. E_T is the maximum transferable energy at 200 keV, E_d is the displacement energy and E_s is the sputtering energy.

^a From Table 4.3 in [1]

^b Calculated from eq. 2 in [3]

Displacement and sputter damages are the most common radiation damages seen in metals and the only way to avoid them is to lower the incident electron energy so that the maximum transferable energy does not exceed the displacement energy. If this is not possible the electron dose should be minimized in order to minimize the damages.

6.2 Damages caused by inelastic electron scattering

Also inelastic scattering can cause damages to the sample. In this section we will consider two of the processes namely specimen heating and radiolysis.

6.2.1 Specimen heating

Specimen heating is caused mainly by phonon vibrations in the material. The main parameters that affect the specimen heating are the beam current and the thermal conductivity of the material. This is shown in **Fig. 6.3** where materials with different thermal conductivity κ (in W/mK) from insulators ($\kappa=0.1$) to good thermal conductors ($\kappa=100$) like metals are represented. In the figure the grey region marks the beam current as measured in the TEM used for the main part of the experiments in this thesis. As can be seen from the figure, beam heating should not be a big problem for these currents. However, if a small particle with good thermal conduction is embedded in a matrix of material with less thermal conductivity, the heating of the particle can be considerable.

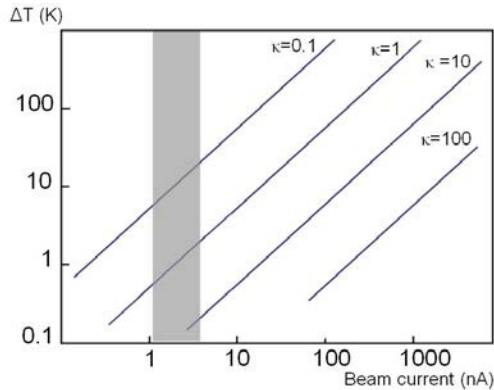


Fig. 6.3 Specimen heating as a function of beam current. The lines marks materials with different thermal conductivity, k (W/mK). The gray region marks the beam current as measured experimentally for the TEM used in this thesis. (Figure reproduced from [1].)

Even if the heating is small it may be enough to increase the diffusivity of particles in the material and thereby induce changes in the structure. Nagase and Umakoshi [5] have for example showed that electron beam induced crystallization shows significant temperature dependence by using MeV electron irradiation on Fe-Zr-B samples at room temperature and below. The best way to avoid heating is by cooling of the sample. This is done using a special holder in the TEM.

6.2.2 Radiolysis

The chemistry and structure of covalent and ionic materials can be changed by radiolysis. In this process an inelastic scattered electron excites an electron in the material to make an interband transition. It is then possible for the electrons and holes to recombine and form an anion vacancy and a cation interstitial. The best

way to reduce radiolysis is to decrease the initial electron-electron interaction. This can be achieved by having thinner samples or higher acceleration voltage.

References

- [1] D.B Williams, C.B. Carter, **Transmission Electron Microscopy: a textbook for materials science, 2nd ed.**, Springer, (2009)
- [2] M.R. McCartney, P.A. Crozier, J.K. Weiss, D.J. Smith, **Electron-beam-induced reactions at transition-metal oxide surfaces**, *Vacuum* 42 (1991) 301-308
- [3] R.F. Egerton, P. Li, M. Malac, **Radiation damage in the TEM and SEM**, *Micron* 35 (2004) 399-409
- [4] T. Nagase, T. Sanda, A. Nino, W. Qin, H. Yasuda, H. Mori, Y. Umakoshi, J.A. Szpunar, **MeV electron irradiation induced crystallization in metallic glasses: Atomic structure, crystallization mechanism and stability of an amorphous phase under irradiation**, *Journal of Non-Crystalline Solids* 358 (2012) 502-518
- [5] T. Nagase, Y. Umakoshi, **Temperature dependence in density-fluctuation-induced crystallization in metallic glass by MeV electron irradiation**, *Intermetallics* 18 (2010) 1803-1808

7 Summary of papers

The papers in this thesis concern the microstructure of transition metal carbides. Both the Ti-Si-C system in **Paper I** and the Nb-C system in **Paper III** have a potential use in electrical contact applications. While **Paper III** focus on relating the structure to electrical and mechanical properties, **Paper I** is based on a more fundamental research to explain the incorporation and segregation of Si in the TiC structure. **Paper II** investigates the structural changes of Nb-Si-C and Zr-Si-C induced by the electron beam in transmission electron microscopy. The Zr-Si-C system was added since we wanted to compare Nb-Si-C with a similar system.

7.1 Paper I

In this paper magnetron sputtered Ti-Si-C films were deposited from elemental targets at a substrate temperature of 350 °C. The voltage on the Si target was changed between the depositions in order to study the incorporation effect of different amounts of Si. It was found that the pure TiC films consisted of substoichiometric TiC_x , with $x \sim 0.7$. When grown on Al_2O_3 (0001) substrates the TiC_x film becomes epitaxial. For up to 5 at.% Si the epitaxy is at least locally sustained and the Si is incorporated in the TiC_x to form an $\text{Ti}(\text{Si},\text{C})$ phase. For an increasing Si content above 5 at.%, the epitaxy is gradually lost and the Si segregates to the column boundaries of the TiC_x grains.

7.2 Paper II

Here the effects of the electron beam in high resolution transmission electron microscopy on the amorphous phase in transition metal silicon carbide are studied. For this purpose, two different transition metals, Zr, and Nb were selected. The electron beam induced formation of crystalline MeC grains in the Nb-Si-C and the Zr-Si-C films. The causes of the crystallization were investigated by studying at the effect of different dose as well as different energy of the electrons in the electron beam. It was found that different beam currents with the same dose generate similar crystallization. If the electron energy is lowered from 200 keV to 80 keV, the crystallization is remarkably reduced for the same dose. The effect of heating was tested by *in-situ* annealing of the sample in the TEM. It was found that the crystallization process started between 400-600 °C. However, this process was much slower than for the beam-induced crystallization. The conclusion is that heating is not the main cause of the crystallization. Instead the energy dependence suggests that the crystallization is produced by a knock-on process where energy from one elastically scattered beam electron is transferred to one of the specimen atoms causing displacement of this atom.

Also, the effect of ion irradiation caused by the ion milling in the sample preparation were investigated by comparing samples made in the conventional way with samples made by the small angle cleavage technique. However, no large difference between the two methods was found.

7.3 Paper III

Nb-C thin films were deposited by unbalanced magnetron sputtering from two elemental targets using a substrate bias of -50 V and a substrate temperature of 300 °C. This resulted in a nanocomposite consisting of crystalline NbC grains surrounded by a matrix of amorphous C. XRD reveals the NbC grains to be of the B1 (NaCl) structure. With an increased C content (from 43 to 64 at.% C) TEM shows a change from grains elongated (~75 nm) in the growth direction to small (3-5 nm) equiaxed grains.

By comparing the areas of the C-C and Nb-C peaks in the C1s spectra the relative amount of amorphous carbon can be calculated from the XPS data. Although an increase of amorphous C with increased C content was found, the surrounding matrix remained at almost the same thickness due to the reduced size of the NbC grains.

The changes in microstructure are found to be similar to those observed in the TiC system. One important difference is the thickness of the matrix, which is much thinner in the case of NbC/a-C compared to TiC/a-C. This can be explained by a larger homogeneity range for TiC, which makes it easier to create C vacancies and therefore allows more free C to cluster during growth. The thinner matrix can be used to explain both the higher hardness and lower resistivity of NbC/a-C compared to TiC/a-C since an a-C matrix softens the structure and is less conducting than the MeC grains.

8 Future work

Investigations of the mechanical and electrical properties of Nb-Si-C are currently ongoing as an expansion to **Paper II** and **Paper III**. These results will be relevant for Nb-C-based coatings as electrical contact material.

One problem with Si in low contact force electrical applications is the formation of oxides, which decrease the contact performance. Ge seems to have less tendency to form oxides and I will therefore investigate the properties of Nb-Ge-C nanocomposites as an alternative to Nb-Si-C. As a replacement of Si, I also intend to look at the Nb-B-C system, since earlier work shows the addition of B into Ti-C coatings to be an interesting alternative as electrical contact material [1].

Although the transition metal carbides show promising results, metals are still the dominant contact materials. One common metal to use is Ag. I would like to investigate how different alloying elements improve corrosion resistance for Ag, by study the reactions including surface composition.

Finally, for the issue of the location of incorporated Si in TiC_x ($x \sim 0.7$), I have initiated a collaboration with computational materials scientists at my department to use ab initio-based methods.

References

- [1] J. Lauridsen, N. Nedfors, U. Jansson, J. Jensen, P. Eklund, L. Hultman, **Ti-B-C nanocomposite coatings deposited by magnetron sputtering**, *Applied Surface Science* 258 (2012) 9907– 9912